Electrostatic gyroscope pull-in study and optimum dimensions using genetic optimization

Hassan E. A. Ibrahim
Electronics and Communication Eng. Dept., College of Eng., and Technology,
Arab Academy for Science and Technology, Cairo, Egypt

Pull-in study of the electrostatic gyroscope is essential for good performance. This paper presents optimum dimensions for the electrostatic actuated gyroscope. Good pull-in performance is obtained using the optimum dimensions. Pull-in analysis is presented for an electrostatic gyroscope. Polynomial algebraic equations for pull-in voltage, pull-in angle, and pull-in torque of the electrostatic gyroscope are presented. Genetic algorithm for choosing the optimum dimensions is presented. New design technique for choosing proper values of the system dimensions is presented, by using genetic optimization. Adequate desired performance is obtained by optimizing the magnitudes of these dimensions.

هذا البحث يقدم دراسة وافية لإستقرار الجيروسكوب فى مرحلة الجذب النهائى. كما يقوم البحث بعرض طريقة لأيجاد القيم المثلى لأبعاد الجيروسكوب ليعطى أداً أفضل فى حالة الجذب النهائى بإستعمال النظام الوراثى لحساب القيم المثلى للجيروسكوب. كما يقدم البحثالمعادلات الجبرية اللازمة لجساب الجهد و ذاوية الدواران والعزم اليكتروستاتيكى والعزم الميكانيكى بشكل عام وبشكل خاص عند مرحلة الجذب النهائى. و قد تم عمل تمثيل للجيروسكوب قبل إستعمال القيم المثلى للإبعاد و تم إعادة التمثيل مرة أخرى بإستعمال القيم المثلى وتم المقارنة بين الحالتين كما تم الحصول على الأدء المطلوب للجيروسكوب عند حالة الجذب النهائى بعد إستعمال القيم المثلى لإبعادة.

Keywords: MEMS, Gyroscope, Genetic, Optimization

1. Introduction

There is a growing interest in micromechanical rates gyroscopes [1-4] due to their small dimensions and their potential of being cheap and yet highly sensitive. Several techniques that can be divided into two main groups are used in order to implement such devices: vibrating [3,4,5] and rotating [4]. The microelectromechanical vibrating rate gyroscopes are classified by their actuation force and the output displacement sensing technique. Several techniques of actuation have been employed so far: electrostatic, either laterally [4] or vertically [5], piezoelectric or electromagnetic [6]. The response to rate due to the Coriolis effect is sensed either capacitively, piezoelectrically or piezoreisitively.

A novel design for a micromachined vibrating ring rate gyroscope is presented [5]. The proposed device uses vertical electrostatic actuation and differential optical sensing to measure the response of the proof mass to rate. This novel microelectromechanical vibrating rate gyroscope does not suffer in principle from cross coupling, electrical or mechanical between the excitation and output modes as opposed to other designs. The theory of the rate gyroscope, including the electromechanical behavior and the optical sensing technique and associated noise sources, which limit performance, is discussed in [5].

There are many examples of MEMS structures, which are actuated by electrostatic forces. These structures include parallel plate, deformable beams or diaphragms, as well as torsion actuators. A set of examples is illustrated in [7-10]. In torsion actuators, in contrast to parallel plate actuators, the plates are tilted and an angle α is defined between the two plates. An important parameter of electrostatic microactuators is the pull-in voltage. In static equilibrium, the electrostatic force/torque and the mechanical force /torque are equal, resulting in a stable condition of the actuator. As the voltage increases, the electrostatic force/torque, resulting in instability or a collapse condition, where a contact between the two plates is formed.

Pull-in analysis has been extensively studied in the literature. In the case of parallel plate actuators, a simple analytical model can

be derived for calculation of the pull-in voltage and pull-in distance [11,12]. Pull-in studies were also carried out for more complicated structures as deformable beams and diaphragms and for torsion actuators [9].

So far, several ways have been employed for estimating the pull-in voltage and pull-in angle for the torsion actuators. The simplest method is using the parallel plate model along with an effective spring torque coefficient of the structure for estimating the pull-in voltage [9,11,12]. This method yields rapid calculations, but shows errors of up to 20%. The conducting plates are restricted to be close to the torsion bar or at the edges of the proof mass.

Pull-in analysis is presented for an electrostatic torsion microactuator in [9]. Two types of microactuators fabricated using bulk micromachining are presented. Measurements done on the fabricated microactuators are reported. In [9] simplified model for calculating the pull-in voltage and the pull-in angle of an electrostatic torsion microactuator is presented. The equilibrium state between the electrostatic and elastic torque is considered, by employing stability considerations.

In this paper, a simplified model for calculating the pull-in angle, pull-in voltage and pull-in electrostatic torque is presented. Extensive simulation has been done for the pull-in performance. Stability consideration has been taken into account by using equilibrium between the electrostatic and mechanical torque by adjusting the operating point. Optimum system dimensions have been calculated by using genetic optimization. The computations are also compared with previously reported results, showing good agreement.

2. Analysis and mathematical model

2.1. System characteristics

The mechanical and electrical behavior of a two-degree of freedom rate gyroscope will be analyzed (confined motion and output mode). Fig. 1 from [9] shows schematic view of the gyroscope including the proof mass, the plates of the capacitors, and the needed parameters for the analysis in the Cartesian frame (*x*, *y*, *z*). In order to model the electrostatic torque, it is assumed that the plates are infinitely wide and they have length *b* in the negative *z* direction. The potential between the plates comes from voltage supply *V*. The Laplace equation of the electrostatic potential between the plates is $\varphi(\varphi)$ and the boundary conditions, in cylindrical coordinates denoted by (*r*, *φ*, *z*).

$$\frac{\partial^2 \phi(\varphi)}{\partial \phi^2} = 0 , \tag{1}$$

where $\phi(\varphi = 0) = 0$, $\phi(\varphi = \alpha) = V$ and V is the applied voltage, α is the angle between the plates, Φ is the electrostatic potential between the plates. Solving (1) yields to,

$$\phi(\varphi) = \frac{V}{\alpha}\varphi . \tag{2}$$

The electrostatic field can be calculated as follows.

$$\vec{E} = -\nabla\phi = \begin{cases} -\dfrac{V}{\alpha r}\hat{\varphi} & \text{between plates} \\ 0 & \text{out of plates} \end{cases} . \tag{3}$$

Where $\hat{\varphi}$ is the unit vector in the direction of *φ*. The charge density ρ_s on the plates is.

$$\rho_S = \varepsilon_o \left(E_{\perp \text{in}} - E_{\perp \text{out}}\right) \Big|_{\phi=0 \text{ or } a} = \pm \frac{\varepsilon_o V}{\alpha r} , \tag{4}$$

where + sign for the upper plate and – for the lower plate. ε_o is the dielectric constant of the vacuum; *r* is the vector of motion. The electrostatic pressure on the upper plate can be calculated.

$$\vec{P}(\alpha) = \int_0^{\alpha} \vec{E}_{\text{upper-plate}} \rho_S d\varphi = -\frac{\varepsilon_o V^2}{2\alpha^2 r^2}\hat{\varphi} . \tag{5}$$

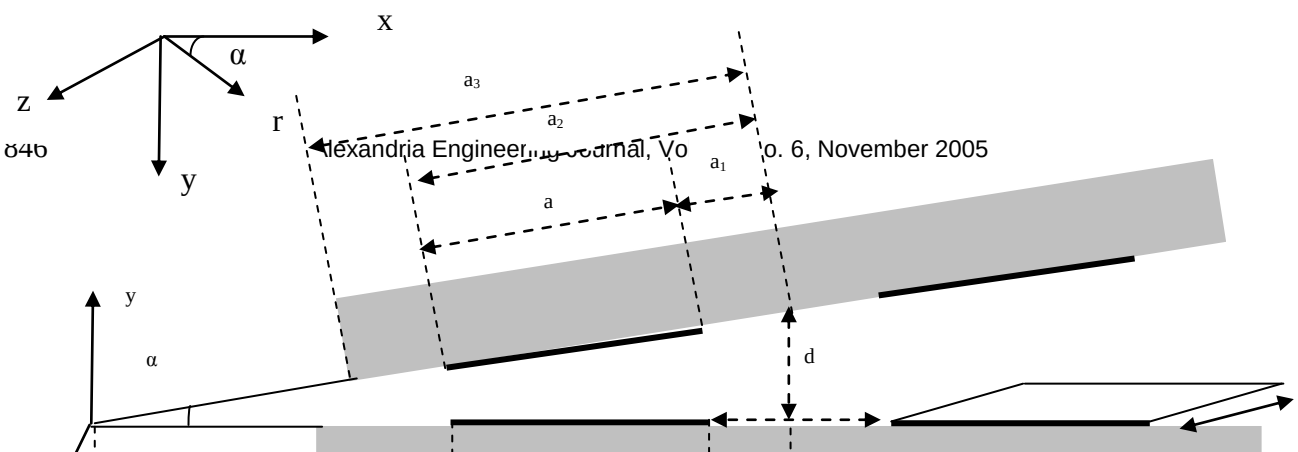

Fig. 1. A schematic view of a gyroscope.

The integration of the plate's elements in the direction of z and r gives the electrostatic torque exerted on one plate where the bottom plate is fixed.

$$\vec{M}(\alpha) = \int_{z=0}^{b} \int_{r=r_1}^{r_2} (r_3 - r)\ \hat{r} \times \vec{P}(\alpha)\ dr dz. \quad (6)$$

The integration of eq. (6) gives the following formula in eq. (7).

$$\vec{M}(\alpha) = \frac{\varepsilon_o V^2 b}{2\alpha^2}\left[\frac{r_3}{r_1} - \frac{r_3}{r_2} + \ln\left(\frac{r_1}{r_2}\right)\right]\hat{z}, \quad (7)$$

where r_1, r_2, r_3, b are defined in fig. 1, and r is the unit vector in the r direction. For more integration accuracy, the electrostatic torque around the z direction has different form in [9] if we assume small angles and infinite plate length b the other form of the electrostatic torque is in eq. (8).

$$\vec{M}(\alpha) = \frac{\varepsilon_o V^2 b}{2\alpha^2}\left[\frac{d}{d - a_2\alpha} - \frac{d}{d - a_1\alpha} + \ln\left(\frac{d - a_2\alpha}{d - a_1\alpha}\right)\right]\hat{z}. \quad (8)$$

From fig. 1, d is the distance between the two plates at the axis of rotation, α_1 is the distance from the axis of rotation the nearest edge of the plate, and α_2 is the distance to the end of the plate, a is the plate length.

Eq. (8) can be modified to the normalized value of the gyroscope angle as in eq. (9).

$$\left|\vec{M}(\alpha)\right| = \frac{\varepsilon_o V^2 b}{2\alpha_{\max}^2}\frac{1}{\theta^2}\left[\frac{1}{1-\beta\theta} - \frac{1}{1-\gamma\theta} + \ln\left(\frac{1-\beta\theta}{1-\gamma\theta}\right)\right]. \quad (9)$$

where

$$\alpha_{\max} = \frac{d}{a_3}\ \beta = \frac{a_2}{a_3}\ \gamma = \frac{a_1}{a_3}\ \theta = \frac{\alpha}{\alpha_{\max}}. \quad (10)$$

Eq. (10) shows that, the electrostatic torque is expressed as a function of the normalized angle θ and the normalization angle α_{max} is determined by the physical structure of the gyroscope.

2.2. Pull-in study

The pull-in state starts when the electrostatic (comes from the applied voltage) torque comes greater than the system inertia then the plates stick to each other. The equilibrium state happens when the electrostatic torque gets equal to opposing mechanical torque; the

system mechanical torque can be represented as:

$$\tau = K_\alpha \alpha \,. \tag{11}$$

As shown from eq. (11) the system mechanical torque is a linear function directly increases with the plate angle α and has a slope K_α, where K_α is the spring torque coefficient. For each gyroscope there is a maximum angle eq. (10), the plates can not turn more than this angle, the gyroscope angle is defined as the tangent of distance between the plates to the length between the centers of the plates to the reference point that stays beyond the proof mass of the proof mass as shown in fig. 1. The angle between the plates is in the range of micro radian, so, for approximation we can neglect the tangent as shown in eq. (10).

The angle of the gyroscope increases with the applied voltage, the angle that the gyroscope operates at is derived from the equilibrium state (i.e. when the electrostatic torque equals to mechanical torque) by solving eq. (12).

$$K_\alpha \alpha = \left|\vec{M}(\alpha)\right| . \tag{12}$$

By solving eq. (9) and eq. (12), an expression for the pull-in voltage as a function of the normalized angle θ can be found as in eq. (13) and (14).

$$V_{pull-in}(\beta,\gamma) = \sqrt{\frac{2K_\alpha d^3}{\varepsilon_o a_3^3 b} f(\beta,\gamma)} \;, \tag{13}$$

$$f(\beta,\gamma) = \frac{\theta_{pin}^3}{\left[\dfrac{1}{1-\beta\theta_{pin}} - \dfrac{1}{1-\gamma\theta_{pin}} + \ln\left(\dfrac{1-\beta\theta_{pin}}{1-\gamma\theta_{pin}}\right)\right]} \;. \tag{14}$$

Then, it can be seen from eq. (13) that, as the applied voltage increases as the normalized angle θ increases, until the normalized angle θ reaches the maximum value and then, the pull-in state starts.

3. Results and simulation

Intensive simulation has been done using MATLAB, the data used for the simulation are listed in table 1 it is taken from practical gyroscope fabricated in [9], [9] presents two types of gyroscope T-type and MMV-type. The data used in this paper that of t-type gyroscope. The table presents the gyroscope dimensions. The results obtained from the simulation are declared as follows.

The simulation of eq. (7) shows the electrostatic torque M comes from the applied voltage V. Fig. 2 shows the electrostatic torque as a function of the gyroscope angle α. The simulation has been done for different applied voltage at (20,15,10,5) V. As shown from fig. 2 as the applied voltage increase as the electrostatic torque increases and, the angle α increases and the pull-in occurs early (at lower α). Fig. 2 shows also the simulation of eq. (11) the gyroscope mechanical torque τ versus the gyroscope angle α, as the gyroscope angle increases as the torque increase linearly, where eq. (11) is linear relationship between the mechanical torque and the angle. For sufficient low voltage, the angle of the proof mass has two physical solutions, where one is stable and the other is unstable (pull-in state). For certain voltage the two solutions coincide. This voltage is defined as the pull-in voltage. For voltage above the pull-in voltage, the electrostatic torque is greater than the mechanical torque for any angle, thus, there are no solution (i.e. no stable operation, pull-in state).

Simulation of eq. (4) is shown in fig. 3, as shown the electrostatic charge grows up as the angle α increases, at the pull-in state the charge increases rapidly, causes the electrostatic torque increases rapidly and the two plates collides, and device goes to malfunction. We can classify the response into three main phases. The first is the acceleration phase, which lasts for the first few micro seconds. During this phase, the charge increases rapidly, and the velocity increases slowly but the position is still close to the initial position. The second phase is

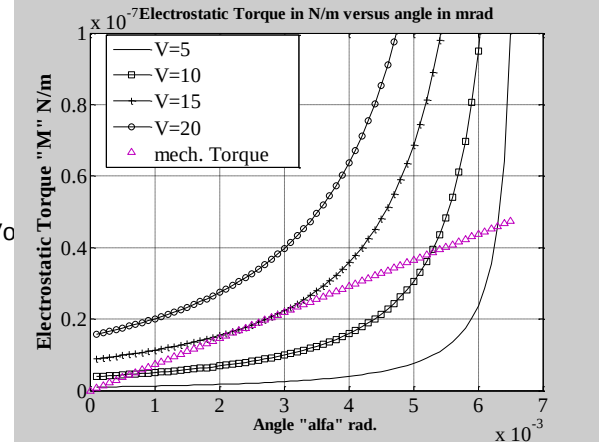

a_2	680 μm
a_3	700 μm
D	4.55 μm
W	31 μm
T	14 μm
L	400 μm
B	1300 μm

Fig. 2. Electrostatic and mechanical torque versus angle α.

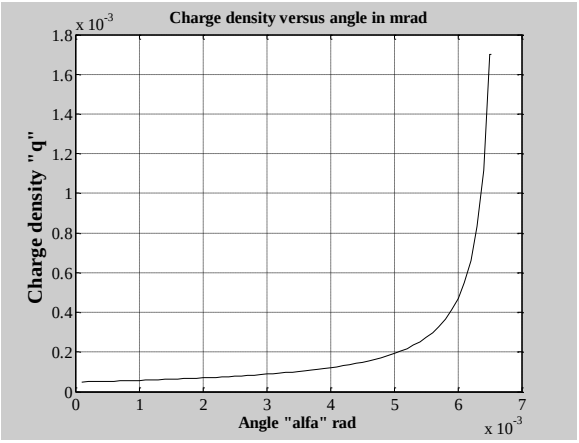

Fig. 3. Charge density versus angle α.

damping phase where the charge and the electrostatic torque are still increasing but at lower rate because of the nonlinearity of the electrostatic torque. The final phase is the pull-in phase; this phase is characterized by rapid increase in the charge and the torque. This rise indicates that there is a sharp spike of current at the moment of pull-in happens when the system is driven from nearly ideal voltage source and this turns out to have important effect on the total amount of energy consumed during the transient. The charge plays big role in the pull-in instability, where controlling the charge control the gyroscope stability.

Simulation of eq. (13), (14) is shown in fig. 4, the pull-in voltage versus the angle α, as the angle increases as the voltage increase,

Table 1
Gyroscope dimensions

System parameters	Value
K_a	$7.3*10^{-6}$
a_1	430 μm

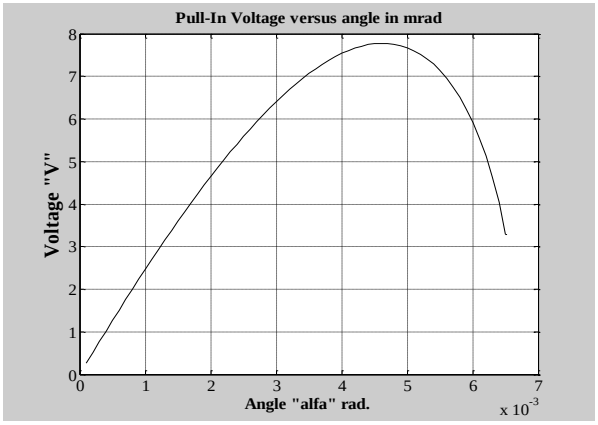

Fig. 4. Pull-in voltage versus angle α.

the pull-in voltage reaches maximum value and then goes down to reach zero at the pull-in state, where short circuit happens and spike occurs between the plates.

A parametric investigation of θ_{pin} dependency on the location parameters β and γ is shown in fig. 5, where the x axis is the γ parameter and the y axis is θ_{pin}, it can be seen that there are no restrictions that are imposed on the location parameters β and γ beside nonphysically values. The pull-in angle can be set in a wide range, from about 0.4 to 1, when the pull-in situation does not occur before the gap is closed. Therefore, a full dynamic range of the gyroscope is achieved; a useful fact in the design of several gyroscope. As shown from fig. 5, as β increases as the pull-in angle increase, and the pull-in angle decreases with increasing γ. It is also known that [9] for lower pull-in voltage, larger plates should be used, but this can result in a lower θ_{pin}. Therefore, careful attention should be paid to design since dynamic range and pull-in voltage are not independent.

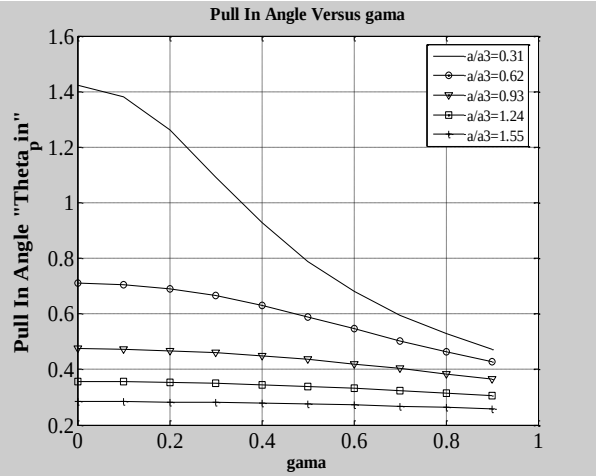

Fig. 5. Pull-in angle versus γ for different β.

As shown from above, we need to increase the pull-in angle θ_{pin} with the lower pull-in voltage by choosing optimum plate's area and optimum value for γ. Where as the plate area increases as the pull-in voltage decreases as shown from eq. (13), (14) and the pull-in angle increases. As γ increases as the pull-in angle decreases and the pull-in voltage decrease. So, we need to implement optimization technique to find the optimum plate area and optimum value for γ to increase the pull-in angle and decrease the pull-in voltage. Genetic optimization can do that; choose the optimum plate area, and optimum value for γ which gives the required pull-in angle and voltage.

4. Genetic algorithm

Genetic algorithm has been implemented to find the optimum values of the plate width b and γ. The procedures for applying the genetic algorithm are found in fig. 6, it starts with wide range of b and γ obtained from design values in [9], at the 1st population pool, computing the fitness for each individual. The fitness is measured towards the maximum pull-in angle and lower pull-in voltage. The 2nd step is sorting the population according to their fitness, and checking for the average fitness, the algorithm stops if converged else goes to the next step. The 3rd step is a death process; eliminate all poor population fitness according to a crossover probability. The 4th step is a crossover process to generate offspring, to keep up the same number in population and to get improved stiffness. The crossover process uses the parents with best fitness, a binary coding is used to express b and γ magnitudes, and with one-point crossover method is used in our case. The 5th step is a mutation, with a mutation probability of 40%, one point mutation is used. Finally, the new population is formed and procedures repeated until reaching the optimal average fitness.

5. Results and simulation for optimum dimension gyroscope

The simulation using the genetic algorithm working on optimum b and γ has been implemented. The fitness function has been worked on increasing the pull-in angle for low pull-in voltage. The optimum values for b= 580 μm and optimum γ = 0.7. Fig. 7 shows the electrostatic torque versus the gyroscope angle α, the electrostatic torque in this graph has applied voltage (10V) and the optimum b and γ, the graph also shows the system mechanical torque represented in eq. (11). As shown from fig. 7 the intersection between the two curves is two points one stable and the other is unstable as discussed above. The other point comes for α = 0.65μ rad. Where for the same applied voltage above in fig. 2 the point of intersection between the electrostatic torque and the mechanical torque was at α = 0.52μ rad. i.e. by changing b and γ the system characteristics and operating point change. The optimum value for b and γ guarantee stable system at the pull-in state. Fig. 8 shows the electrostatic torque and mechanical torque versus the angle α using optimum b and γ. It is done to make it easy to be compared with fig. 2 to show the effect of using the optimum values on the system operating point, pull-in voltage and pull-in angle.

Fig. 9 shows the pull-in voltage for the gyroscope using the optimum values versus the angle α. as shown the pull-in voltage has been decreased. For different pull-in angles. It can be compared with fig. 4 to see the different when using the optimum dimension parameters.

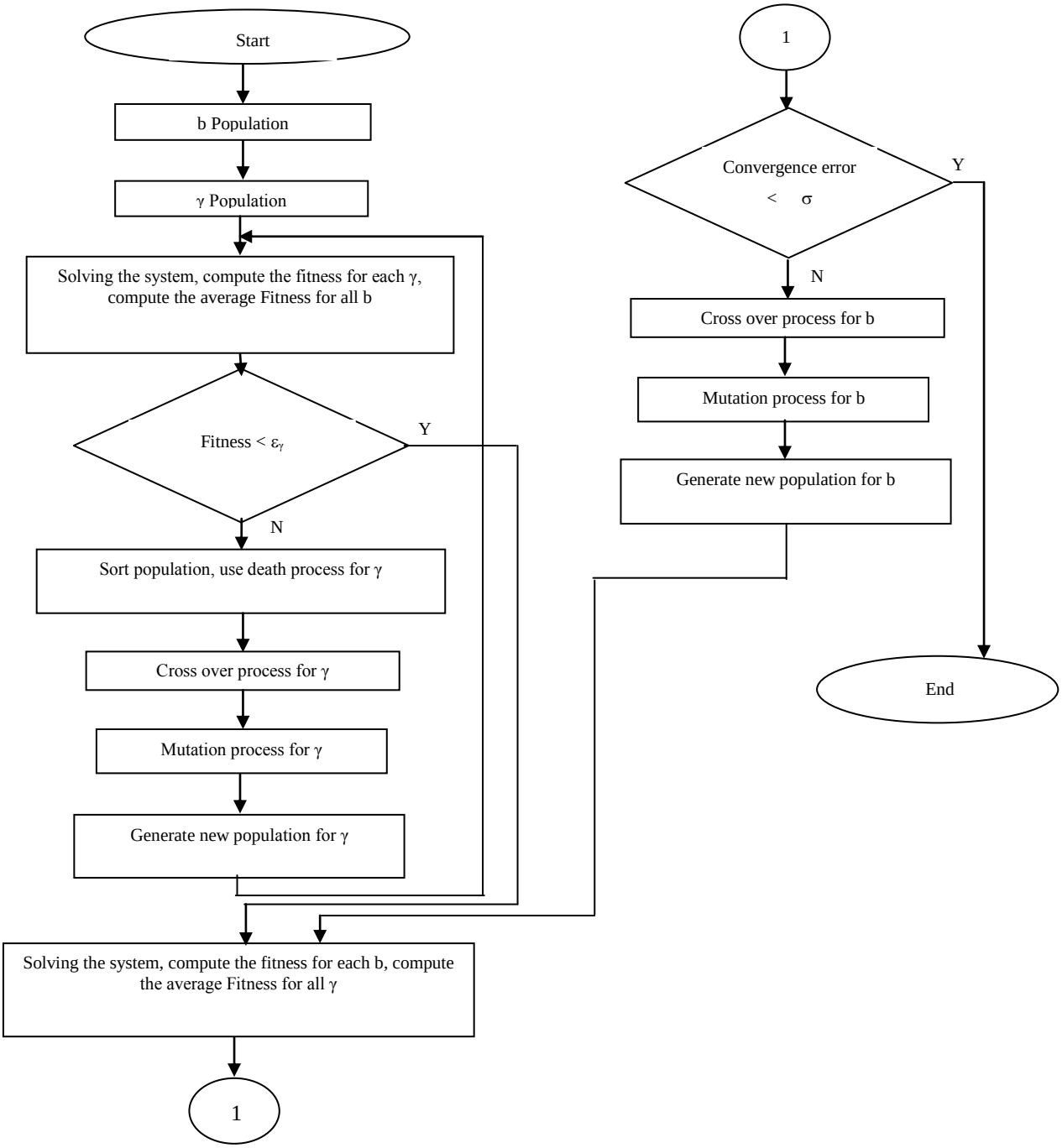

Fig. 6. Genetic algorithm flowchart.

6. Conclusions

Gyroscope analysis has been presented with optimization objective in mind. Gyroscope model is presented and simulated Using MATLAB. Device electrostatic and mechanical torque, pull-in voltage and angle, charge density, effect of device dimension on these parameters are investigated. The simulation gave us conclusion that, the gyroscope dimensions *b* and *γ* have big effect on the system pull-in stability. When the plate's area increases the pull-in voltage decreases and the

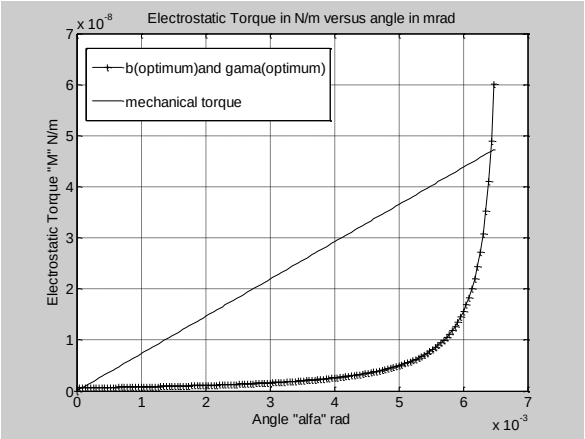

Fig. 7. Electrostatic and mechanical torque versus angle α using optimum b and γ.

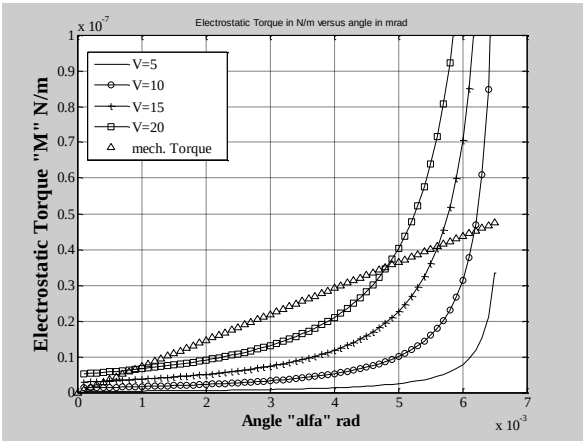

Fig. 8. Electrostatic and mechanical torque for different applied voltages versus angle α using optimum b and γ.

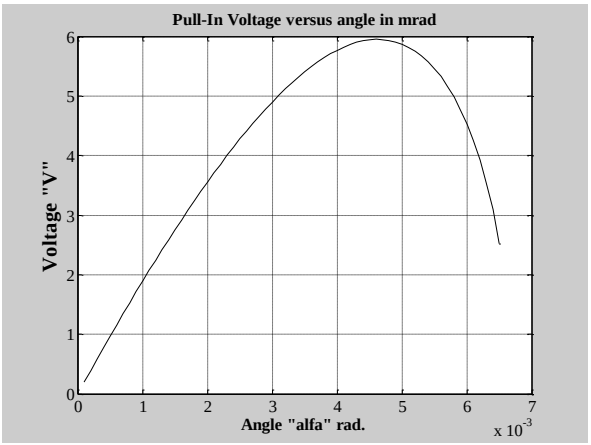

Fig. 9. Pull-in Voltage versus angle α using optimum b and γ.

pull-in angle increases. When γ increases pull-in voltage decreases and the pull-in angle decreases. Genetic optimization algorithm has been implemented to find the optimum value for the plat area and γ. The system has been simulated using the optimum value for b and γ. Then, comparison has been discussed after using the optimum parameters in the simulation. The results using the optimum value for b and γ were much better, where they give better device pull-in stability than using the nominal value for b and γ obtained from nominal design methods.

References

[1] J. Bernstein, S. Cho, A. King, A. Kourepenis, P. Maciel, and Weinberg, "A micromachined Comb-Drive Tuning Fork Rate Gyroscope", IEEE Microelectromechanical Systems Workshop, Ft. Lauderdale, FL, Feb. 7-10, pp. 143-148 (1993).

[2] J. Soderkvist, "Micromachined gyroscopes", Sens. Actuators A, Vol. 43, pp. 65-71 (1994).

[3] M. Putty and K. Najafi, "A Micromachined Vibrating Ring Gyroscope", in Solid-State Sensors and Actuators Workshop, pp. 213-220 (1994).

[4] K. Tanaka, Y. Mochida, M. Sugimoto, K. Moriya, T. Hasegawa, K. Atsuchi, and K. Ohwada, "A Micromachined Vibrating Gyroscope", Sens. Actuators A, Vol. 50, pp. 111-115 (1995).

[5] Ofir Degani, Dan J. Seter, Eran Socher, Shmuel Kaldor, and Yael Nemirovsky, "Optimal Design and Noise Consideration of Micromachined Vibrating Rate Gyroscope with Modulated Integrative Differential Optical Sensing", JMEMS IEEE, Vol. 7 (3), pp. 329-338 (1998).

[6] F. Paoletti, M.A. Gretillat, and N. F. de Rooij, "A Silicon Micromachined Vibrating Rate Gyroscope with Piezoresistive Detection and Electromagnetic Excitation", JMEMS IEEE, Workshop, Switzerland, pp. 162-167 (1996).

[7] G. Florence Marc-Alexix G. and F. Nicolaas De Rooij, "Improved Design of a Silicon Micromachined Detection and

Electromagnetic Excitation", JMEMS IEEE, Vol. 8 (3), pp. 243-249 (1999).

[8] P. Sungsu and H. Roberto, "Adaptive Control for the conventional Mode of Operation of MEMS Gyroscopes", JMEMS IEEE, Vol. 12 (1), pp. 101-108 (2003).

[9] Ofir Degani, Eran Socher, Ariel Lipson, Tomer Leitner, Dan J. Seter, Shmuel Kaldor, and Yael Nemirovsky, "Pull-in Study of an Electrostatic Torsion Microactuator", JMEMS IEEE, Vol. 7 (4), pp. 373-379 (1998).

[10] J. Barry, Gallacher, John Hedley, James S. Burdess, Alun James Harris, Alexandria Rickard, and David O. King, "Electrostatic Correction of Structural Imperfections Present in Microring Gyroscope", JMEMS IEEE, Vol. 14 (2), pp. 221-234 (2005).

[11] R.K. Gupta and S.D. Senturia, "Pull-in Time Dynamics as a Measure of Absolute Pressure", in Proc. IEEE Int. Workshop on Microelectromechanical Systems (MEMS'97), Nagoya, Japan, 26-30, pp. 290-294 (1997).

[12] W.C. Tang, T.C.H. Nguyen, M.W. Judy, and R.T. Howe, "Electrostatic Comb-Drive of Lateral Polysilicon Resonators", Sensors and Actuators, A, Vol. 21 (1-3), pp. 328-331 (1990).

[13] K.F. Man, K.S. Tang, S. Kwong and W.A. Halang," Genetic Algorithms for Control and Signal Processing", ISBN 3-540-76101-2 Springer-Verlag Berlin Heidelberg, New York.

[14] Mitsuo Gen Runwei Cheng, "Genetic Algorithms and Engineering Optimization", John Wiley and Sons Inc., New York (2000).

Received August 1, 2005
Accepted October 29, 2005